Supplementary Information

Immobilization of Ca^{2+} by OH^- ions on calcium silicate hydrates

Ziga Casar[1,2,3*], Laura Mismetti[1,2], Maya Harris[1], H. Chris Greenwell[2], Karen Scrivener[1], Milan Předota[4], Paul Bowen[1]

[1]Laboratory of Construction Materials, Institut des Matériaux, Ecole Polytechnique Fédérale de Lausanne (EPFL), CH-1015 Lausanne, Switzerland.
[2]Department of Chemistry, Durham University, South Road, Durham, DH1 3LE, United Kingdom.
[3]Department of Civil and Environmental Engineering, Princeton University, Princeton, NJ 08544, United States.
[4]Department of Physics, Faculty of Science, University of South Bohemia, Branišovská 1760, 370 05 České Budějovice, Czech Republic.

*Corresponding author(s). E-mail(s): casar.ziga@outlook.com;

Contents

1 Segmented flow tubular reactor (SFTR) synthesis

The SFTR consisted of a 40 m long coiled tube with an internal diameter of 4 mm.

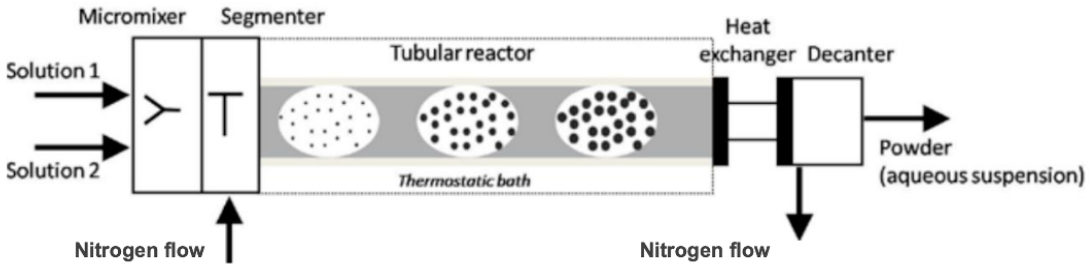

Fig. S1 Diagram of the segmented flow tubular reactor (SFTR) [1, 2].

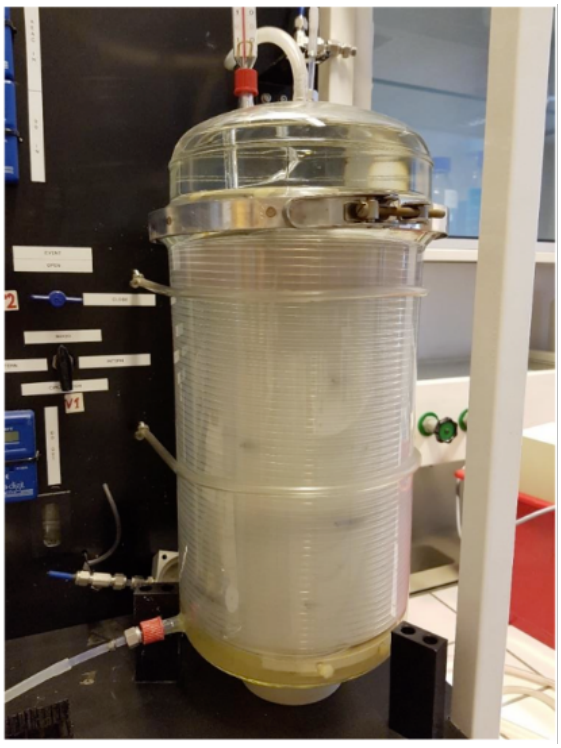

Fig. S2 Picture of the SFTR.

Ca/Si	[Ca]	[Si]	10 M NaOH
1	0.055 M	0.05 M	2 mL
1.25	0.065 M	0.05 M	4 mL
1.5	0.080 M	0.05 M	12 mL
1.75	0.095 M	0.05 M	15 mL
2	0.110 M	0.05 M	20 mL

Table S1 Reactant composition for synthetic C-S-H in the SFTR reactor. The total volume of the SFTR was 800 mL.

Fig. S3 Synthetic C-S-H produced in the segmented flow tubular reactor (SFTR) after filtration (left) and freeze-drying (right).

2 X-ray diffraction

X-ray powder diffraction was carried out by a PANalytical X'pert X-ray diffractometer with an X'celerator detector with double bounced monochromatic CuK_{α} radiation. Wet and dry C-S-H samples were prepared through the back-loading process, in which the sample holder was loaded from the rear and placed on a rotating sample stage. The patterns were recorded between 5°-70° (2Θ) with a fixed divergence slit of $\frac{1}{2}$ and a step size of 0.017° for 30 min. XRD was used to observe the intrinsic C-S-H peaks at 29.4, 32.1, and 50.1 ± 0.1° [3], as well as any secondary phases.

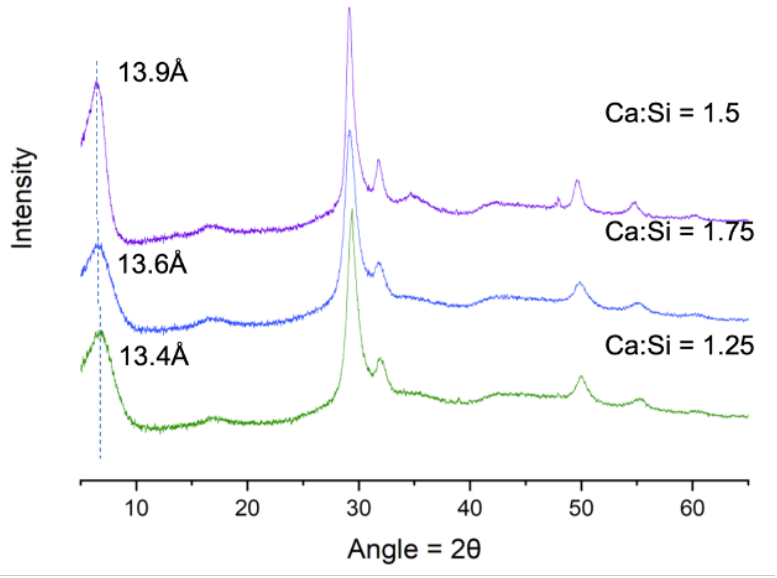

Fig. S4 X-ray diffraction (XRD) patterns of SFTR-produced freeze-dried samples. The annotations show the d-spacing of the 002 reflection which is attributed to the layer spacing of C-S-H.

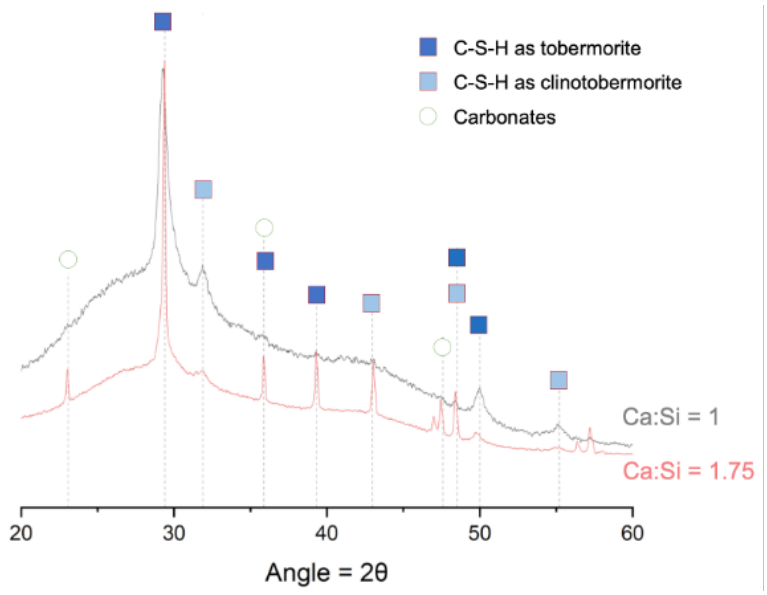

Fig. S5 X-ray diffraction (XRD) pattern of wet and filtered C-S-H with Ca/Si = 1 and 1.75 after final dispersion in 10 mM NaOH (full symbols in Figure 1C). The XRD pattern shows typical C-S-H reflections, suggesting no alteration to the mainlayer nanofoil structure. The presence of carbonates in Ca/Si = 1.75 sample is attributed to the handling of the sample (exposure to air).

3 Transmission electron spectroscopy

The transmission electron microscope (TEM) used was the Tecnai Osiris TEM, supplied with field emission imaging (FEI). The microscope was operated at 200 kV in the TEM mode for diffraction analysis. To prepare a sample for TEM, 0.15 g of filtered wet C-S-H was dispersed in 20 mL of isopropanol supplied by Reactolab S.A. (99%). The samples were placed into an ultrasonic bath for 15 min, and one drop of the dispersion was placed on a carbon film 300 mesh grid, supplied by Electron Microscopy Sciences. The sample on the grid was enclosed in a glass petri dish and allowed to dry for 20 h under a lamp.

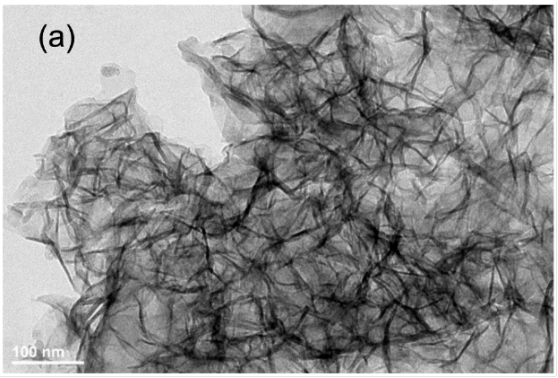

Fig. S6 TEM micrograph of synthetic C-S-H with Ca/Si = 1.5.

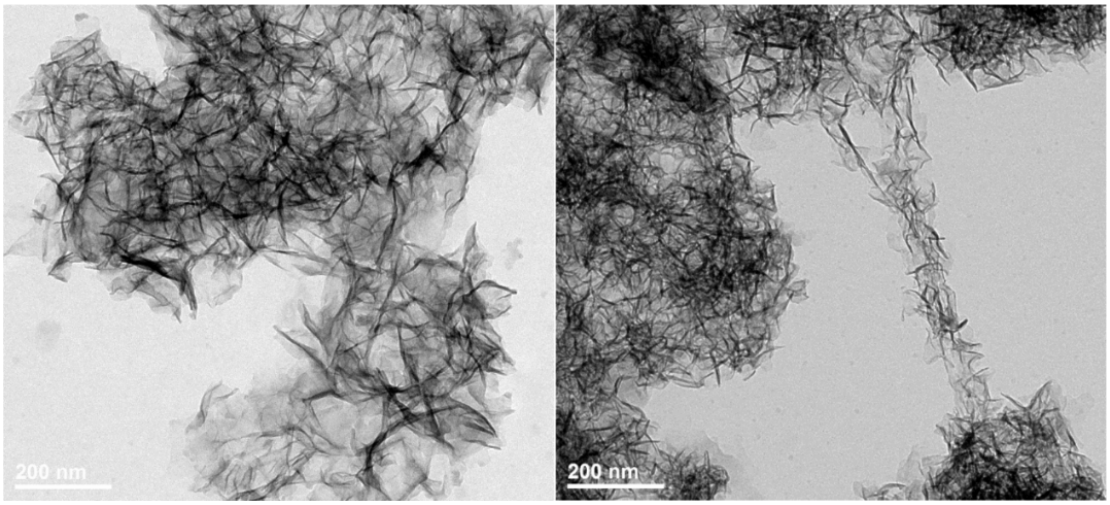

Fig. S7 TEM micrographs of synthetic C-S-H with Ca/Si = 1.7.

Reactant Ca/Si	Measured Ca/Si (ICP-OES)	Ca [mmol/L]	Si [mmol/L]	Na [mmol/L]
1.7	1.79	2.64	0.50	289.7
1.8	1.88	4.89	0.66	272.7
1.9	2.05	5.06	0.59	347.1
2	2.3	6.98	0.58	340.2

Table S2 ICP-OES measured concentrations for C-S-H with Ca/Si = 1.7-2.0, supernatant compositions at pH 12 for high Ca/Si samples.

4 Inductive coupled plasma – optical emission spectroscopy (ICP-OES)

The supernatant compositions for C-S-H with Ca/Si between 1.7 and 2.0 are shown in Table S2 and were used as input parameters for thermodynamic modeling with which the aqueous speciation at equilibrium at a pH 12 was calculated (Figure S8). Thermodynamic modeling was carried out with PhreeqC and the Cemdata 18, C-S-HQ, and LLNL databases [4–8].

The measured Ca/Si are higher than the targeted reactant Ca/Si for all samples, which is in agreement with previous studies on high Ca/Si C-S-H [3]. Thermodynamical modeling (Figure S8) shows an increase in the concentration of Ca^{2+}, $Ca(OH)^{+}$, $CaSiO_3$, and $CaNO_3{}^{+}$ with an increase in the Ca/Si ratio. Contrary to Ca/Si = 1.7 to 1.9, at Ca/Si = 2.0 an increase in $NaHSiO_3$ and $HSiO_3{}^{-}$ species, and the appearance of the $CaHSiO_3{}^{+}$ species are observed. Ca^{2+} remains the dominant species over the entire range of Ca/Si ratios. This is consistent with the Pourbaix diagram (logC-pH) of a 2.5 mM calcium solution which states a prevalence of Ca^{2+} over $CaOH^{+}$ and $Ca(OH)_{2,aq}$ below pH 12.6 (Figure S9) [9]. However, Figure S8 shows that the relative amount of $Ca(OH)^{+}$ in comparison to Ca^{2+} increases with an increase in Ca/Si, therefore with an increase in pH. The relatively higher proportions of $Ca(OH)^{+}$ at increased Ca/Si and the discrepancy between thermodynamically calculated (that does not account for surface complexations) and ICP-OES measured concentrations suggests increased co-adsorption rates of Ca^{2+} and OH^{-} at the surface and therefore increased zeta potential values, as theorized by Casar et al. [10, 11].

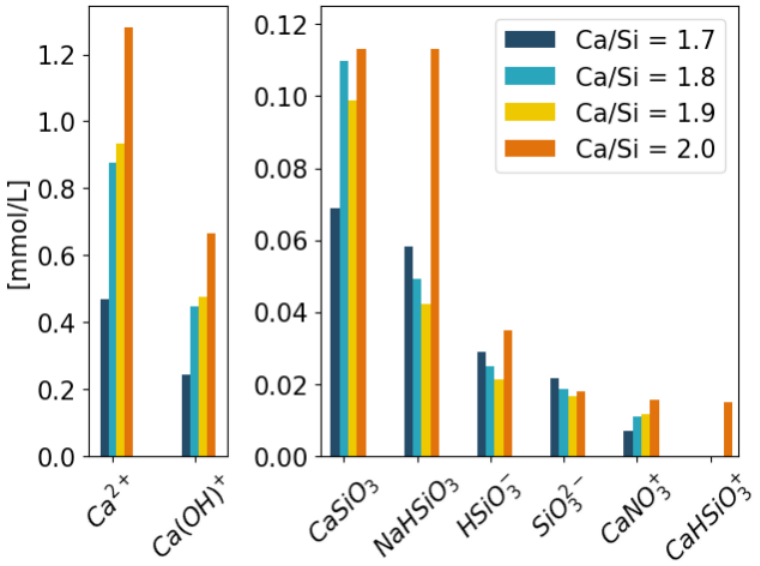

Fig. S8 Aqueous speciation calculated by PhreeqC with Cemdata 18, C-S-HQ, and LLNL databases comparing synthetic C-S-H reaction supernatants for Ca/Si = 1.7-2.0 at pH 12.

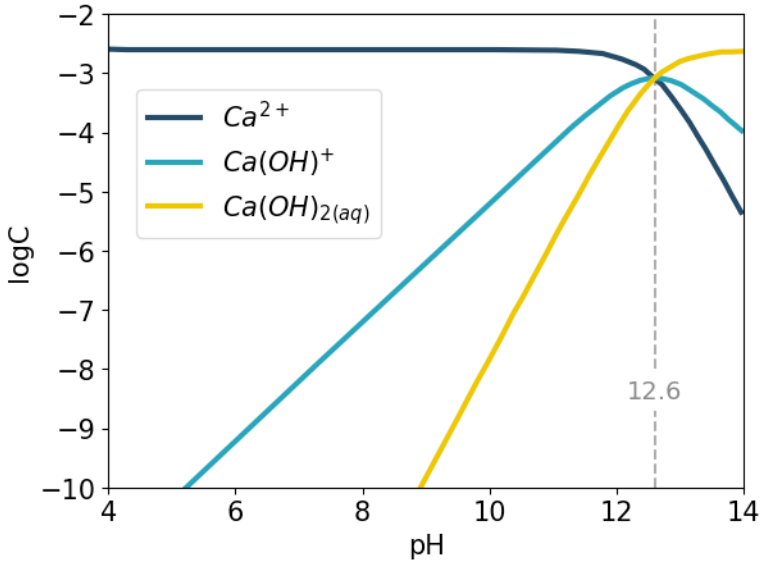

Fig. S9 Pourbaix diagram of a 2.5 mM calcium solution [9].

5 Molecular Dynamics

The surface silicate chains were modeled with a mean chain length of 3 (i.e. 75% of bridging Q^{2b} silicates were vacant), which is an expected value for C-S-H with Ca/Si $\sim$ 1.5 synthesized with the direct precipitation method [3, 12].

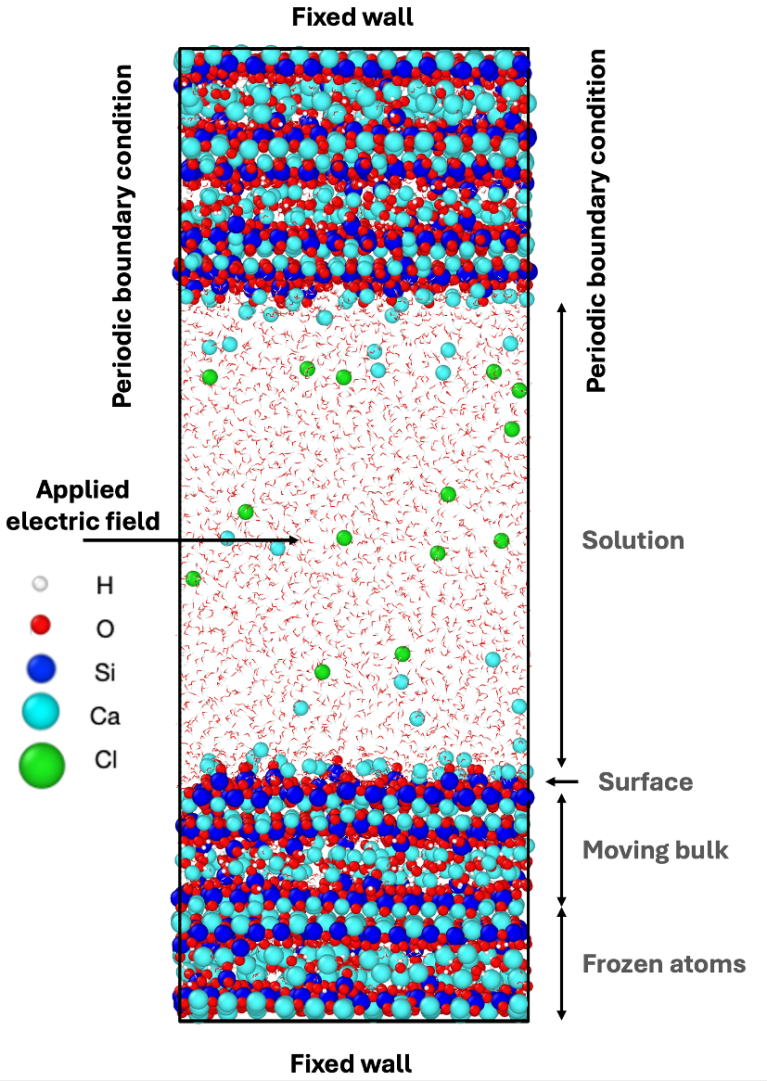

Fig. S10 Simulation box for non-equilibrium molecular dynamics (NEMD).

The interatomic forces were modeled with the CementFF4 force field [13]. The force field uses a polarizable description of silicate oxygens, with which the structure of calcium silicate hydrates is accurately predicted [13, 14]. Due to the size limitation of the simulation box, it is not possible to

OH^- ions/nm^2	Number of $Ca(OH)_2$ units added to each surface
0	0
0.32	2
0.64	4
1.13	7

Table S3 Number of added $Ca(OH)_2$ units per surface in the simulated C-S-H systems.

model the exact concentration of OH^- ions for pH 12. At pH 12 the molarity of the OH^- ions equals 0.01 M (approximately 1 OH^- ion per 5500 H_2O molecules). Such low ionic concentrations result in poor sampling statistics and, therefore, require large simulation times [15, 16]. While at pH 13 the OH^- molarity equals 0.1 M (1 OH^- per 550 H_2O molecules) and, therefore, would be possible to simulate, the limitation occurred due to the formation of calcium-hydroxide ion complexes and 'prenucleation clusters' [9]. At these solution conditions, the precipitation of calcium hydroxide occurs [3, 17] and was seen in our simulations (not shown here) as the formation of mentioned calcium-hydroxide ion solution complexes and 'prenucleation clusters'. These solution complexes and clusters adsorbed at the C-S-H surfaces, therefore changing the anion molarity of the solution. Consequently, a comparison between different Ca^{2+}-OH^- adsorption concentrations at constant solution conditions was impossible.

Since MD simulations with explicit OH^- ions at pH 12 were impossible due to solution concentration limitations, and at pH 13 impossible due to the formation of solution complexes and clusters, the selected solution anionic species was Cl^-. Ca^{2+} ions under the simulated conditions interact weekly with Cl^- ions and therefore do not form complexes. Cl^- ions allowed us to compare different effective surface charges, arising from the co-adsorption of Ca^{2+} and OH^- ions, at equal solution anionic concentration, as in our experimental measurements.

The systems were equilibrated for 10 ns in the NPT ensemble at 1 atm and 297.15 K with periodic boundary conditions in all axes directions. A 50 ns non-equilibrium molecular dynamics (NEMD) run followed in the NVT ensemble with fixed-wall conditions in the z-axis direction. Finally, an 11.2 ns NEMD run was carried out from which the mean values were obtained. Further details are given in the main text and the LAMMPS input files are provided as part of the supplementary information.

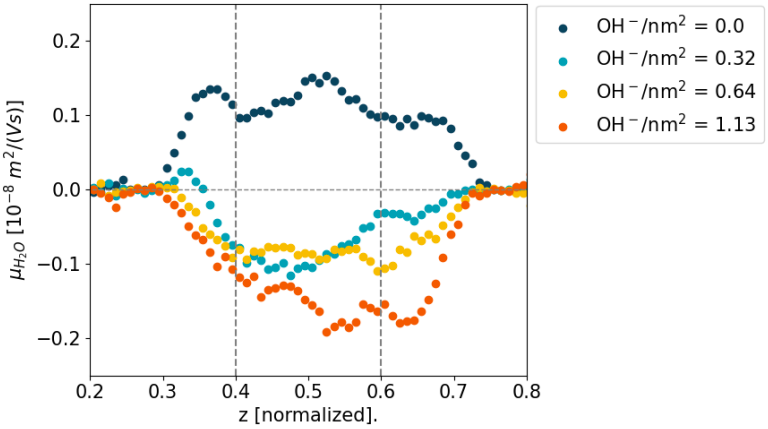

Fig. S11 Water mobilities profile averaged over 5.6 ns. The average water mobility value of bulk solution for calculating zeta potentials (Equation 1) was taken between positions 0.4 and 0.6 of normalized z-axis.

The zeta potential is calculated using the Helmholtz-Smoluchowski equation:

$$\zeta = -\frac{\eta\mu}{\varepsilon_0\varepsilon_r} \tag{1}$$

where [18]:

- $\eta = 9.8\ 10^{-4} Pa \cdot s$ is the experimental bulk water dynamic viscosity
- μ is the average water mobility in bulk solution (Figure S11)
- $\varepsilon_r = 79$ is the experimental bulk water relative permittivity
- ε_0 is the vacuum permittivity

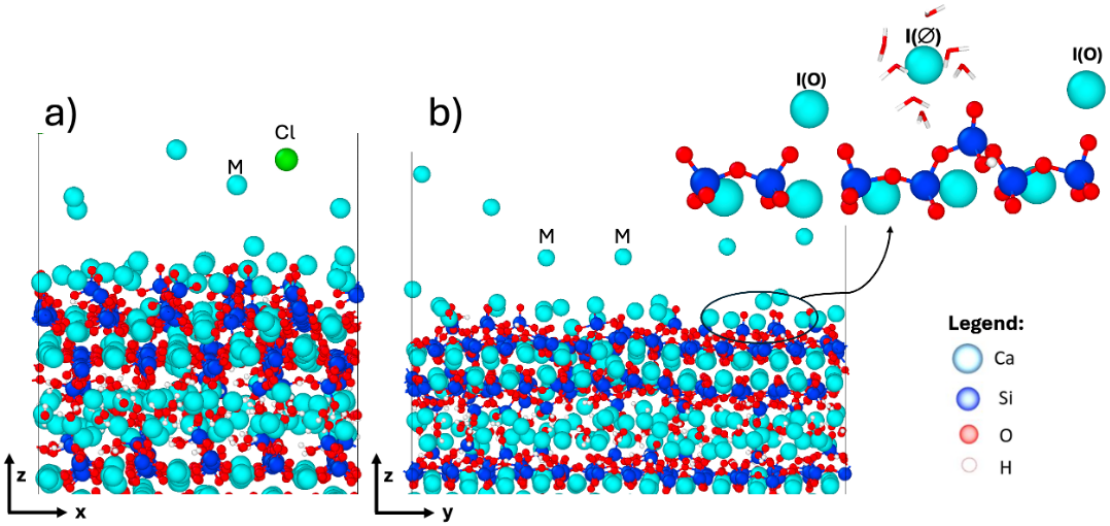

Fig. S12 C-S-H surface with $OH^-/nm^2 = 0$. Annotations show the respective Ca^{2+} sites as categorized by their mobility and coordination environment. Water molecules, except of I(∅ - outer sphere adsorbed immobile Ca^{2+}), are hidden for clarity.

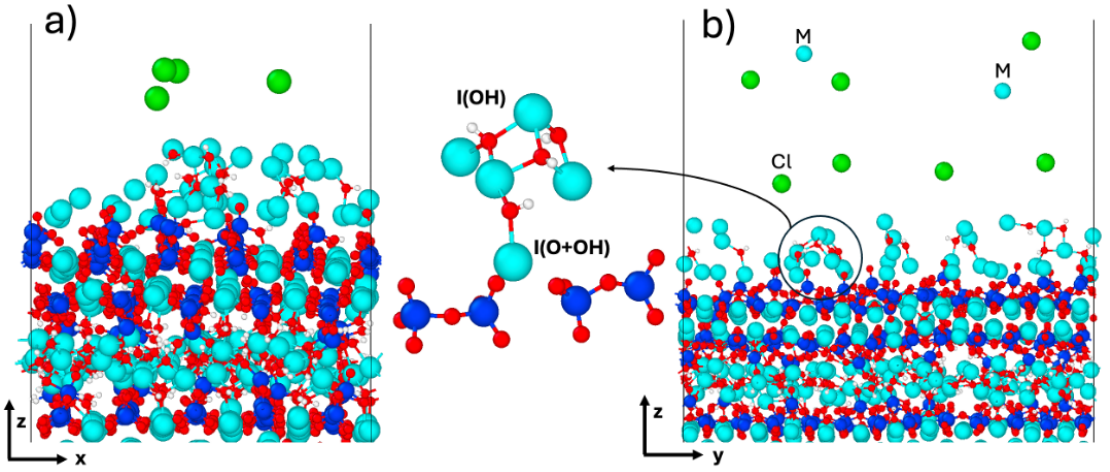

Fig. S13 C-S-H surface with $OH^-/nm^2 = 1.13$. Annotations show the respective Ca^{2+} sites as categorized by their mobility and coordination environment. Ca^{2+} - OH^- coordination is shown with bonds. Water molecules are hidden for clarity.

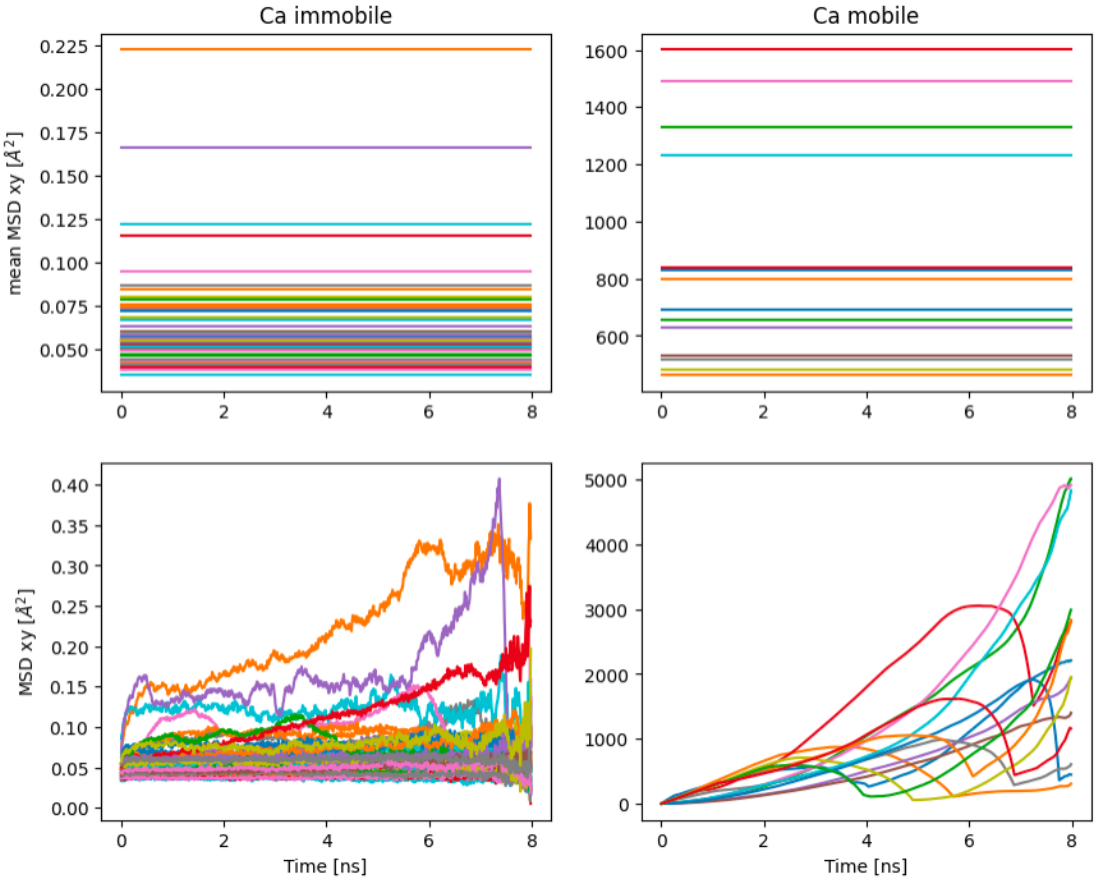

Fig. S14 Mean square displacement (MSD) of individual solution Ca^{2+} ions (immobile and mobile).

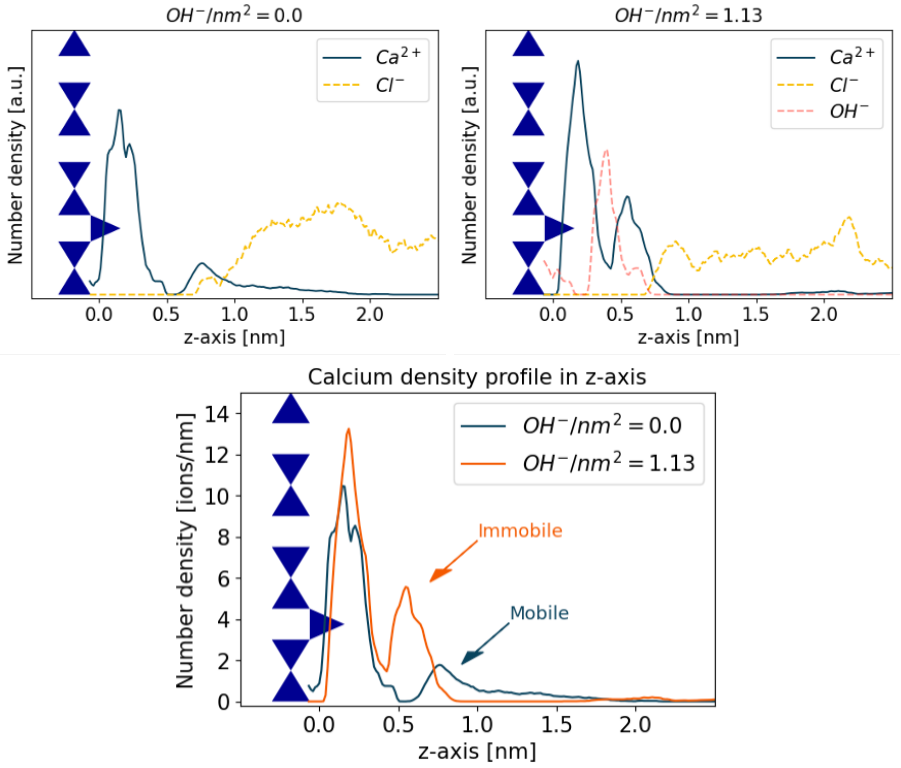

Fig. S15 Density profiles for Ca^{2+}, OH^- and Cl^-.

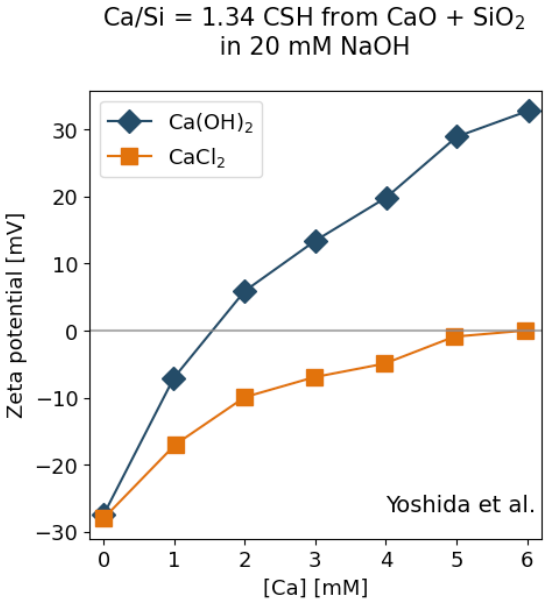

Fig. S16 Measured zeta potential of Ca/Si = 1.34 in 20 mM NaOH solution titrated with $Ca(OH)_2$ and $CaCl_2$ as reported by Yoshida et al. [19].

6 C-S-H nanofoil model

Assuming a 3 layer, 2 interlayer thick C-S-H nanofoil with MCL = 3 where all vacant silicate bridging sites of the interlayer are occupied by Ca^{2+} ions, and with additional Ca^{2+}/dimer = 0.73 calcium packing of the interlayer [10, 11], then such a nanofoil would have the Ca/Si ratios predicted in Table S4, depending on the adsorbed amount of calcium ions at the surface. Moretails are given in the manuscript and in in references [10, 11].

Surface adsorbed Ca^{2+}/nm^2	Ca/Si ratio of the nanofoil	Proportion of calcium atoms at the surface $[Ca_{Surf}/Ca_{Total}]$
0	1.33	0%
3.6	1.55	14.3%
7.2	1.77	24.9%
10.8	1.99	33.2%

Table S4 Increase of Ca/Si of the nanofoil due to surface adsorption of Ca^{2+}.

References

[1] Jongen, N. *et al.* Development of a continuous segmented flow tubular reactor and the "scale-out" concept – in search of perfect powders. *Chemical Engineering & Technology* **26**, 303–305 (2003).

[2] Aimable, A. *et al.* Precipitation of nanosized and nanostructured powders: Process intensification and scale-out using a segmented flow tubular reactor (sftr). *Chemical Engineering & Technology* **34**, 344–352 (2011).

[3] Harris, M., Simpson, G., Scrivener, K. & Bowen, P. A method for the reliable and reproducible precipitation of phase pure high ca/si ratio (>1.5) synthetic calcium silicate hydrates (csh). *Cement and Concrete Research* **151**, 106623 (2022).

[4] Andalibi, M. R. *et al.* On the mesoscale mechanism of synthetic calcium–silicate–hydrate precipitation: a population balance modeling approach. *J. Mater. Chem. A* **6**, 363–373 (2018).

[5] Kulik, D. A. *et al.* Gem-selektor geochemical modeling package: revised algorithm and gems3k numerical kernel for coupled simulation codes. *Computational Geosciences* **17**, 1–24 (2013).

[6] Lothenbach, B. *et al.* Cemdata18: A chemical thermodynamic database for hydrated portland cements and alkali-activated materials. *Cement and Concrete Research* **115**, 472–506 (2019).

[7] Wagner, T., Kulik, D. A., Hingerl, F. F. & Dmytrieva, S. V. Gem-selektor geochemical modeling package: Tsolmod library and data interface for multicomponent phase models. *The Canadian Mineralogist* **50**, 1173–1195 (2012).

[8] Hummel, W., Berner, U., Curti, E., Pearson, F. J. & Thoenen, T. Nagra/psi chemical thermodynamic data base 01/01. *Radiochimica Acta* **90**, 805–813 (2002).

[9] Ruan, Y. *et al.* Effects of metal ions on the flotation of apatite, dolomite and quartz. *Minerals* **8** (2018).

[10] Casar, Z. *et al.* Pycsh: Automated atomic-level structure generation of bulk c-s-h and investigation of their intrinsic properties. *Cement and Concrete Research* **183**, 107593 (2024).

[11] Casar, Z., Kunhi Mohamed, A., Bowen, P. & Scrivener, K. Atomic-level and surface structure of calcium silicate hydrate nanofoils. *The Journal of Physical Chemistry C* **127**, 18652–61 (2023).

[12] Kumar, A. *et al.* The atomic-level structure of cementitious calcium silicate hydrate. *The Journal of Physical Chemistry C* **121**, 17188–17196 (2017).

[13] Casar, Z. *et al.* Cementff4: Formal atomic charge polarizable force field for cementitious systems – bulk and surface. *Cement and Concrete Research* **187**, 107708 (2025).

[14] Valavi, M., Casar, Z., Kunhi Mohamed, A., Bowen, P. & Galmarini, S. Molecular dynamic simulations of cementitious systems using a newly developed force field suite erica ff. *Cement and Concrete Research* **154**, 106712 (2022).

[15] Předota, M., Machesky, M. L. & Wesolowski, D. J. Molecular origins of the zeta potential. *Langmuir* **32**, 10189–10198 (2016).

[16] Biriukov, D., Fibich, P. & Předota, M. Zeta potential determination from molecular simulations. *The Journal of Physical Chemistry C* **124**, 3159–3170 (2020).

[17] Samanta, A. *et al.* Synthesis of Nano Calcium Hydroxide in Aqueous Medium. *Journal of the American Ceramic Society* **99**, 787–795 (2016).

[18] Mamontov, E. *et al.* Dynamics and Structure of Hydration Water on Rutile and Cassiterite Nanopowders Studied by Quasielastic Neutron Scattering and Molecular Dynamics Simulations. *The Journal of Physical Chemistry C* **111**, 4328–4341 (2007).

[19] Yoshida, S., Elakneswaran, Y. & Nawa, T. Electrostatic properties of c–s–h and c-a-s-h for predicting calcium and chloride adsorption. *Cement and Concrete Composites* **121**, 104109 (2021).